Predicting spiral wave patterns from cell properties in a model of biological self-organization

Daniel Geberth* and Marc-Thorsten Hütt
Computational Systems Biology, School of Engineering and Science, Jacobs University, Bremen 28759, Germany
(Received 13 May 2008; revised manuscript received 2 July 2008; published 23 September 2008)

In many biological systems, biological variability (i.e., systematic differences between the system components) can be expected to outrank statistical fluctuations in the shaping of self-organized patterns. In principle, the distribution of single-element properties should thus allow predicting features of such patterns. For a mathematical model of a paradigmatic and well-studied pattern formation process, spiral waves of cAMP signaling in colonies of the slime mold *Dictyostelium discoideum*, we explore this possibility and observe a pronounced anticorrelation between spiral waves and cell properties (namely, the firing rate) and particularly a clustering of spiral wave tips in regions devoid of spontaneously firing (pacemaker) cells. Furthermore, we observe local inhomogeneities in the distribution of spiral chiralities, again induced by the pacemaker distribution. We show that these findings can be explained by a simple geometrical model of spiral wave generation.

DOI: 10.1103/PhysRevE.78.031917 PACS number(s): 87.18.Hf, 87.18.Vf

I. INTRODUCTION

Spiral wave patterns are abundant in biological systems. They emerge from the interacting units of the system in a self-organized manner. While it is relatively easy to explain the existence of propagating wave fronts (target patterns) and spiral waves in excitable media from the properties of the excitable system (see, e.g., Ref. [1]), it requires additional model assumptions to explain the establishment of spiral waves starting from an initially homogeneous system (see, e.g., Refs. [2–4]). Particularly for *Dictyostelium discoideum* (Dd.) pattern formation this question has been studied intensely over the last two decades.

Dd. is widely used as a model system of biological pattern formation [5], self-organization [1], and developmental programs [6]. Features of the Dd. life cycle have been studied, for example, from the perspective of cell sorting [7], relation between cAMP receptor affinity and patterns [8], as well as by assessing the role of the various components in the intracellular signaling pathway and the feedback loop involving cAMP with respect to pattern formation and the route toward a multicellular aggregate [9,10]. Recent research experimentally showed that cell properties (e.g., the response strength to a chemotactic signal) remain rather constant in time for single cells but vary strongly throughout a population of cells [11].

In all this richness, Dd. pattern formation is predominantly an intensely studied example of biological self-organization, where the patterns emerge from the interacting units of the system. In contrast to many physical systems, where local fluctuations determine the details of the pattern, we can here expect the composition and spatial distribution of cell properties to translate into features of the spatiotemporal pattern. This observation suggests the intriguing possibility of predicting the outcome of the pattern formation process from a detailed inventory of cellular properties.

There are several models on how heterogeneity is created in the cAMP signaling system of Id. Goldbeter *et al.* assume that cells follow a genetically determined developmental path, and then show that an initial spread of cells on this path (due to the lack of synchronization of the cell cycle or other sources of heterogeneity) leads to spiral wave formation [2]. A competing model by Levine *et al.* identified a local genetic feedback mechanism as the critical amplifying ingredient, which translates small heterogeneities due to random spontaneous firing events into fully developed spiral waves [3]. Palsson *et al.* include the dynamics of the inhibitor (PDI) of phosphodiesterase (PDE), an agent degrading cAMP, and track the selection for spiral waves (as opposed to target waves) to random secretions of PDI [4]. The competition between spiral waves and target waves is also of critical importance for the formation of cAMP patterns in Dd. [12].

Remarkably, the influence of the genetic feedback loop (which is made explicit in Refs. [3,4] and implicitly underlies the developmental path of Ref. [2]) on large-scale properties of the patterns has been realized only recently by Sawai *et al.* [10]. They modeled Dd. mutants lacking or overexpressing certain components of the internal feedback loop by using different feedback strengths, and found that, both in the simulations and in the mutant data, the average density of spiral waves depends on the feedback strength. They also were the first to apply the phase singularity method (originally introduced by Gray *et al.* and Bray *et al.* [13,14] in the context of heart tissue dynamics) to the tracking of spiral waves in Dd.

Here we focus on one specific model of Dd. pattern formation, which in the past has been very successful in providing insight into the link between the cellular properties and the observed spatiotemporal patterns, namely, the one developed in Refs. [3,9] and recently employed by Sawai *et al.* [10]. In contrast to Ref. [10], we assume a fixed pattern of spontaneously firing (pacemaker) cells and try to predict the probabilities of finding the tips of spiral waves at any given spatial point in the cell colony.

II. THE MODEL

The Dd. signaling model considered here is the one introduced by Levine *et al.* [3,9] and later slightly modified by

*d.geberth@jacobs-university.de

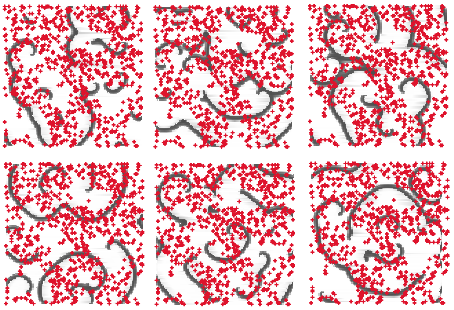

FIG. 1. (Color online) Snapshots of the asymptotic spiral state of several realizations of identical initial conditions on a 100 $\times$100 grid, differing only in the seed of the random number generator. Dark color denotes areas of high cAMP concentration, red +indicate pacemaker positions. On the level of a few single runs, there is no obvious connection between the pacemaker locations and the cAMP pattern.

Sawai *et al.* [10]. Its dynamic variables are the extracellular cAMP concentration c and the excitability E representing the responsiveness of cells to outside cAMP stimulation at a given discretized position. Each grid point corresponds to a single cell or small cluster of cells. The dynamic variables are governed by (see also Ref. [10])

$$\dot{c}_{ij} = -\Gamma c_{ij} + r_F s_{ij}(t) + DL_{ij}(c) \tag{1}$$

and

$$\dot{E}_{ij} = \eta + \beta c_{ij}, \tag{2}$$

where $\Gamma = 8\ \mathrm{min}^{-1}$ is the rate of external cAMP degradation, $r_F = 300\ \mathrm{min}^{-1}$ is the cAMP secretion rate of firing cells, $D = 2.3 \times 10^{-7}\ \mathrm{cm}^2/\mathrm{sec}$ is the cAMP diffusion constant, β is the feedback from cAMP concentration to excitability, and η is the autonomous increase of excitability over time. All results shown here were obtained with $\beta = 0.2$ and $\eta = 0$ unless explicitly stated otherwise. $L_{ij}(c)$ is a discretized Laplace operator realized by a 3×3 matrix M (convolution kernel) acting on the ijth element and its Moore neighborhood

$$L_{ij}(c) = \sum_{k=1}^{3} \sum_{l=1}^{3} M_{kl} c_{i+k-2, j+l-2}, \tag{3}$$

with

$$M = \begin{pmatrix} 1/2 & 1/2 & 1/2 \\ 1/2 & -4 & 1/2 \\ 1/2 & 1/2 & 1/2 \end{pmatrix}.$$

Other convolution kernels M can be used, but for us the above choice minimized discretization artifacts in the geometric shape of the excitation fronts on the relevant time and size scales. The cAMP wave fronts in Fig. 1 tend toward diamond shapes, other discretized Laplace operators tend toward square shapes [cf. Fig. 4(d) of Ref. [10]] or octagons; these tendencies are amplified by the feedback loop and strongly regularize the shape of the excitability fronts, which is an unwanted artifact that becomes more pronounced with growth of an excitable area. The excitability E is initialized at zero and then rises monotonically until it hits $E_{\max} = 0.93$, where it remains fixed. The two mentioned model variants (Ref. [3] vs [10]) differ (except for parameter settings) essentially in the sources and sinks allowed for E. We integrated these equations using an explicit Euler scheme with step size $\Delta t = 0.01$ minutes, the grid spacing corresponds to $\Delta x = 0.06$ mm, as in Ref. [10].

The additional discrete rules governing the state of the cell are summarized in the state matrix $s_{ij}(t)$, where essentially $s = 0$ if the cell is quiescent or refractory, and $s = 1$ if the cell is firing. Using $\tau \in [-T_{\mathrm{ARP}}, T_{\mathrm{RRP}}]$, the exact changes to the state matrix over one excitation cycle can be written as follows. Assume a cell has just entered the absolute refractory phase (ARP) after firing; set $\tau = -T_{\mathrm{ARP}}$ and $s = 0$. After T_{ARP}, the cell enters the relative refractory phase (RRP), where re-excitation is possible at a decreasing threshold level; $0 \leqslant \tau \leqslant T_{\mathrm{RRP}}$ and $s = 0$. If the excitation threshold governed by

$$t_{ij}(\tau) = \left[c_{\max} - A \frac{\tau}{\tau + T_{\mathrm{ARP}}} \right] (1 - E_{ij}) \tag{4}$$

[with $c_{\min} = 4$, $c_{\max} = 100$, $T_{\mathrm{ARP}} = 2$ min, $T_{\mathrm{RRP}} = 7$ min, and $A = (T_{\mathrm{RRP}} + T_{\mathrm{ARP}})(c_{\max} - c_{\min})/T_{\mathrm{RRP}}$] is surpassed by the local cAMP concentration c_{ij}, the cell starts firing; set $s_{ij} = 1$. If on the other hand the end of the RRP is reached without firing, the cell enters the ready state; keep τ constant at $\tau = T_{\mathrm{RRP}}$, which results in $t_{ij} = c_{\min}(1 - E_{ij})$. The firing state $s_{ij} = 1$ lasts for $T_F = 1$ min, after which the cell reenters the ARP, and the excitation cycle repeats as described above.

In order to initiate the signaling process, it is necessary to introduce sources of excitation, which is commonly accomplished by letting some cells fire spontaneously (pacemaker cells). In order to study the systematic shaping of patterns by cell properties, we assume pacemakers to be fixed cells (in contrast to Ref. [10]) that receive a small chance $p_F = 0.002$ to fire in each computational (Euler) time step they spend in the ready state. The assumption of fixed pacemakers is biologically motivated by the distribution of cell properties at the beginning of a real experiment: the cells are usually not synchronized with respect to their cell cycle, and starvation also does not set in at exactly the same time across the cell colony. Therefore it is not unreasonable to assume some cells (or small clusters of cells) to start signaling spontaneously, while the rest is still passive (see Ref. [15]). Note that the exact (temporal) firing pattern of pacemakers introduces a random element that can drastically alter the asymptotic state (i.e., the dynamic but quasistationary pattern of fully developed spirals) even for fixed starting conditions in the dynamic variables (Fig. 1).

In order to track the position of spiral wave tips, we used the phase singularity method introduced by Gray *et al.* and Bray *et al.* [13,14]. We checked that spiral tips typically do not meander far from their initial location in this model, hence we calculated the time average of spiral tip occupancy for every grid point.

III. RELATIONSHIP OF PACEMAKER POSITION TO SPIRAL POSITION DISTRIBUTION

As we pointed out above, the random firing of pacemaker cells can greatly alter the resulting asymptotic pattern. Figure

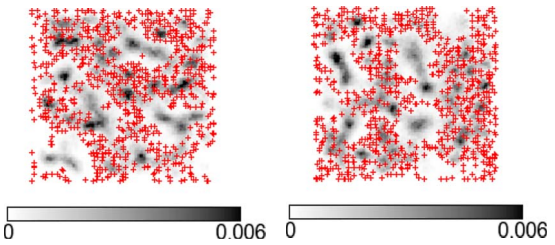

FIG. 2. (Color online) Average of the spiral tip occupancy of 1000 numerical runs, for the pacemaker distribution from Fig. 1 left) and one alternative pacemaker distribution (right). Dark color now denotes areas of high average spiral tip occupancy and red crosses indicate pacemaker positions. The statistical anticorrelation of spiral tip positions and pacemaker locations becomes visible.

1 illustrates this fact with snapshots of the asymptotic state from six numerical runs on a 100×100 grid, differing only in the firing pattern of pacemaker cells. On the single run level, there is no obvious connection between the pacemaker positions (indicated as red +) and the positions of spiral tips. However, looking at the average spiral tip occupancy of 1000 runs (Fig. 2), one discovers an anticorrelation between pacemaker positions and spiral tip occupancy; spiral tips of many runs cluster in areas of low pacemaker density, while there is no discernible systematics to the spiral tips lying in areas of high pacemaker density. Note that while the somewhat heterogeneous pacemaker patterns in Fig. 2 were chosen to highlight the anticorrelation, the same holds for homogeneously distributed pacemaker patterns. The correlation coefficient between the pacemaker positions and spiral occupancy shows a growing anticorrelation over pacemaker density (data not shown), mainly owing to the increasing statistical significance.

IV. MINIMAL MODEL WITH THREE PACEMAKERS

The anticorrelation of pacemaker positions and spiral tips can be understood by means of a simple geometrical model based on the mechanism of spiral formation we observe in this system. Most known mechanisms for the formation of spiral waves from planar or circular waves, such as, e.g., cross field stimulation [16], rely on some sort of obstacle that breaks the wave in such a way that one or two open ends are created that then curl up into spiral waves. The typical scenario of spiral formation in the present model is subtly different. In the following, we give a description of the mechanism and how it leads to the observed nontrivial spiral tip statistics.

Because of the positive feedback from cAMP concentration to excitability, pacemaker cells are surrounded by growing regions of high excitability that allow the propagation of waves (Fig. 3, $t=1$ and $t=2$). Each consecutive wave extends the excitable area by cAMP diffusing into the unexcitable surroundings. Once two excitable regions connect, the combined excitable area is dominated by one pacemaker, the other pacemaker is enslaved. If i and j are pacemakers with identical *a priori* firing probabilities λ per time step and respective observed average firing frequencies f_i and f_j, the probability for i to dominate j is given by

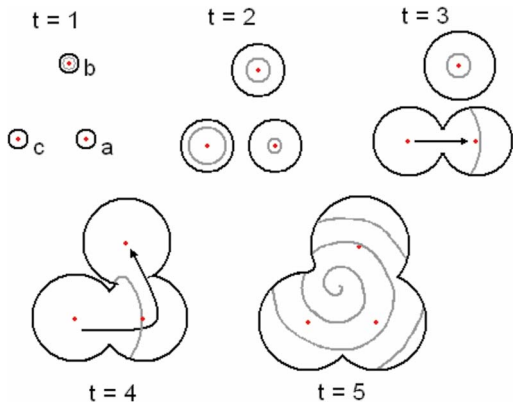

FIG. 3. (Color online) Schematic mechanism of spiral formation driven by unexcitable inner region between areas of high excitability. When two initially independent regions driven by one pacemaker each ($t=1$, $t=2$) are connected, one of the pacemakers is enslaved ($t=3$). Subsequent connection with a third region can cause the creation of a spiral wave ($t=4$, $t=5$) with the spiral tip coming to rest somewhere in the initially unexcitable inner area between the pacemakers.

$$p(i\to j)=\frac{f_i}{f_i+f_j}\exp\left(-\frac{d_{ij}}{v_W}\lambda\right)+\frac{1}{2}\frac{f_i}{f_i+f_j}\left[1-\exp\left(-\frac{d_{ij}}{v_W}\lambda\right)\right]+\frac{1}{2}\frac{f_j}{f_i+f_j}\left[1-\exp\left(-\frac{d_{ij}}{v_W}\lambda\right)\right],\tag{5}$$

where d_{ij} is the distance between the pacemakers and v_W is the wave velocity. The first term describes the case when i fires and the subsequent wave travels to j and enslaves j before j fires. The second and third term describe the cases where either i or j emit a wave that is intercepted by a wave from the other pacemaker. Since the *a priori* firing probabilities are identical, it is assumed that in these cases each pacemaker has a 50% chance of eventually dominating the other. Because a firing event directly translates into a constant amount of radial growth of the excitable region (neglecting curvature effects in the early phase), the firing frequencies in Eq. (5) can be replaced by the radii of the excitable regions at the moment of contact.

If a third pacemaker is positioned similarly to b in Fig. 3, an unexcitable area can be enclosed between the pacemakers. If the pacemaker dominating the figure-of-eight area of a and c also dominates the third region by bridging the far gap first ($t=4$), the waves emanating from it will curve around the obstacle in the middle, creating a closed excitable loop region. If the circumference on the inside of the loop is long enough, cells can recover enough to be reexcitable when the wave hits them again, giving rise to a curved wave traveling in a circle. Because of the radius difference, the wave starts curling up more tightly on the inside, forming a spiral once the unexcitable region in the middle has become excitable, with the spiral tip being located somewhere in the initially unexcitable region ($t=5$ in Fig. 3, corresponding to case I in Fig. 4).

This mechanism is subtly different from cross field stimulation and other known methods of spiral formation, insofar

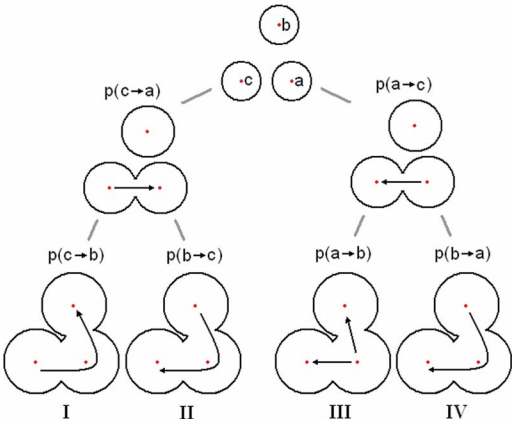

FIG. 4. (Color online) Decision tree showing the four possible wave patterns resulting from the connection of three initially independent pacemaker areas (top) in a given temporal order imposed by the pacemaker firing pattern. In this scheme, the *a*-*c* connection happens first, with the combined area being dominated by one or the other (center row). Once the second connection is formed (bottom row), four possible patterns emerge. The probabilities for each case are determined by the observed firing frequencies as deduced from the radius constellation at the time of each connection. The geometric shape of the triangle formed by the pacemakers obviously plays an important role; assume *b* was far to the right, making the interior angle at *a* very large and the ones at *b* and *c* very small. For almost all radius constellations, this pacemaker arrangement would yield a rod-shaped combined pulsing region dominated by one of the pacemakers, since there would be no sufficiently big unexcitable inner area to curve around.

that only the action of one pacemaker is required to trigger the formation of a spiral wave from an arrangement of excitability fronts. There is no requirement for temporal proximity to other firing events, since the wave fronts responsible for creating the areas of high excitability to not directly interact. Compared to obstacle-driven spiral formation, where two open wave ends and hence two spirals are created behind the obstacle, here typically only one spiral is formed.

For a given connection order imposed by the pacemaker firing pattern, there are essentially four options for the resulting wave pattern, as shown in Fig. 4, for the case where first the *a* and *c* regions and then the *a* and *b* regions connect. These can be summarized as right handed spirals, left handed spirals, and pulsing regions dominated by one pacemaker.

The probability of getting a right handed spiral (here defined as having positive orientation; the spiral tip corresponds to the finger tips of a curled right hand) is given by case I in Fig. 4,

$$p_+ = p(c \to a)p(c \to b), \tag{6}$$

the probability for a left handed spiral is given by cases II and IV,

$$p_- = p(c \to a)p(b \to c) + p(a \to c)p(b \to a). \tag{7}$$

These are not necessarily identical, which makes it interesting to not only look at the total probability of getting a spiral

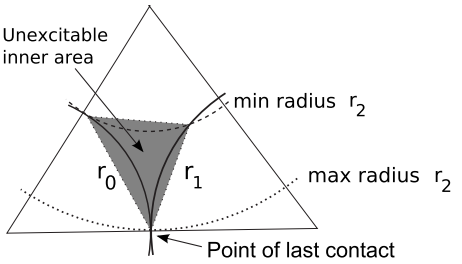

FIG. 5. Schematic of the geometric construction underlying our spiral probability prediction algorithm. The unexcitable area indicated in gray here is for r_2 equal to the minimum value required to ensure the chosen point of last contact is indeed the last contact. The unexcitable area is shown triangular, because the shortest route for a wave curving around this obstacle is given by straight lines.

$$p_{\text{tot}} = p_+ + p_- \tag{8}$$

but also at the chirality asymmetry

$$A = p_+ - p_-. \tag{9}$$

The probabilities (8) and (9) depend on the specific radius constellation. So far, we have not yet succeeded in finding closed expressions for the ensemble averages over all possible radius constellations, which would amount to a spatial probability density for these quantities, depending only on the geometrical placement of the pacemakers. However, the following algorithm for traversing all relevant radius constellations yields a good approximation for the situation involving three pacemakers (see Fig. 5).

Going along the edges of the triangle formed by the pacemakers in small steps Δs, consider each point to be the "point of last contact," where a closed excitable ring has just been formed. This fixes the two solid radii r_0 and r_1. We used $\Delta s = 0.1\Delta x$ to get a smooth distribution.

For all possible radii for the remaining pacemaker area r_2 which ensure the point previously chosen is indeed the last contact and at the same time allow a nonzero unexcitable inner area to be formed, find the corresponding unexcitable inner area. The step size for r_2 is again Δs.

Going backwards in time and correspondingly reducing all radii, reconstruct the radius constellations when the second and first connections happened and calculate the probabilities (8) and (9) by adding up the probabilities leading to cases I, II, and IV in Fig. 4 in the appropriate way.

Multiply this probability with the probability of observing this specific radius constellation (see below) and normalize by the size of the inner area (because only one spiral is formed, and it could come to rest anywhere in that area). All points in the unexcitable inner area determined above are weighted with this number and added to the grand total.

Repeating these steps for all radius constellations yields the predicted average spiral occupancy for every grid point inside the triangle.

In order to only take configurations into account that can really yield spiral waves, we impose the additional requirement that the circumference C_I of the unexcitable inner area (assumed to be triangular, a linear connection of the circle-circle intersection points of the radii) must be sufficiently

large to allow cells to recover enough to be reexcitable after the wave has traveled around the obstacle. More specifically, we require that $C_I \geqslant 3/2 d_R$, where $d_R = v_W \tau_C$ is the distance that a wave front can travel during the critical recovery time that just barely allows reexcitation. Since the excitability inside the excitable regions is practically saturated, this distance can be read off as the distance between consecutive waves in established spirals (see Fig. 1), $d_R \approx 25\Delta x$. The factor 3/2 takes into account that the initial firing event leading to the spiral reaches all boundaries of the excitable region it originates in simultaneously. Hence, only the two other regions are available as recovery "time" for the cells that will be first reached by the wave after it curved around the obstacle. However, because wave speed is strongly reduced when going around corners because of higher wave curvature (see, e.g., Ref. [17]), we found that $d_R \approx 12\Delta x$ and hence $C_I \geqslant 18\Delta x$ is a better criterion.

We estimate the expected number of firing events $\bar{n}$ as the average of all three participating pacemakers, which can be deduced from the radii, since $r_i \approx n_i \Delta r$, where Δr is the radial growth of the excitable area per firing event. From our observations, Δr varies approximately logarithmically with the feedback strength β for $0.005 \leqslant \beta \leqslant 0.2$,

$$\Delta r \approx a \ln(\beta) + b \tag{10}$$

with $a \approx 0.37$ and $b \approx 2.06$ (data not shown). We assume a Gaussian distribution of firing events with mean $\bar{n}$ and standard deviation $\sqrt{\bar{n}}$,

$$p(r) = \frac{\Delta s}{\sqrt{2\pi\bar{n}}} \exp\left(- \frac{\left(\frac{r}{\Delta r} - \bar{n} \right)^2}{2\bar{n}} \right). \tag{11}$$

The probability of obtaining a given radius constellation is then

$$p_C = p(r_0) p(r_2) \tag{12}$$

since only one of the two radii fixed by the initial requirement of "last contact" is independent.

The outcome of this algorithm is a remarkably good prediction of the result obtained by averaging over several thousand simulations of the minimal situation with three pacemakers. Figure 6 shows a comparison of the prediction and our simulations for two triangular pacemaker arrangements. The anticorrelation of pacemaker position and spiral tip occupancy agrees with our initial impression from Fig. 2. The total spiral probability p_{tot} is highest in regular triangles, since there the likely case of similar observed firing frequencies for all pacemakers favors radius constellations with large unexcitable inner areas (total spiral probability in simulation integrated over area indicated by red circle: 12.8% vs 11.5% in prediction). In more asymmetric triangles, similar observed frequencies lead to smaller unexcitable inner areas located near the boundary of the triangle that are often not sufficient for spiral creation (simulation: 8.4% vs 6.8% in prediction).

In addition, our geometric model predicts a spatial unmixing of chiralities along the longest edge of the triangle. This predicted chirality asymmetry is supported by the numerical simulation (Fig. 6, bottom row). In regular triangles the asymmetry of each vertex almost cancels out with the identical asymmetries from the other two vertices, leading to a diminished degenerate asymmetry pattern.

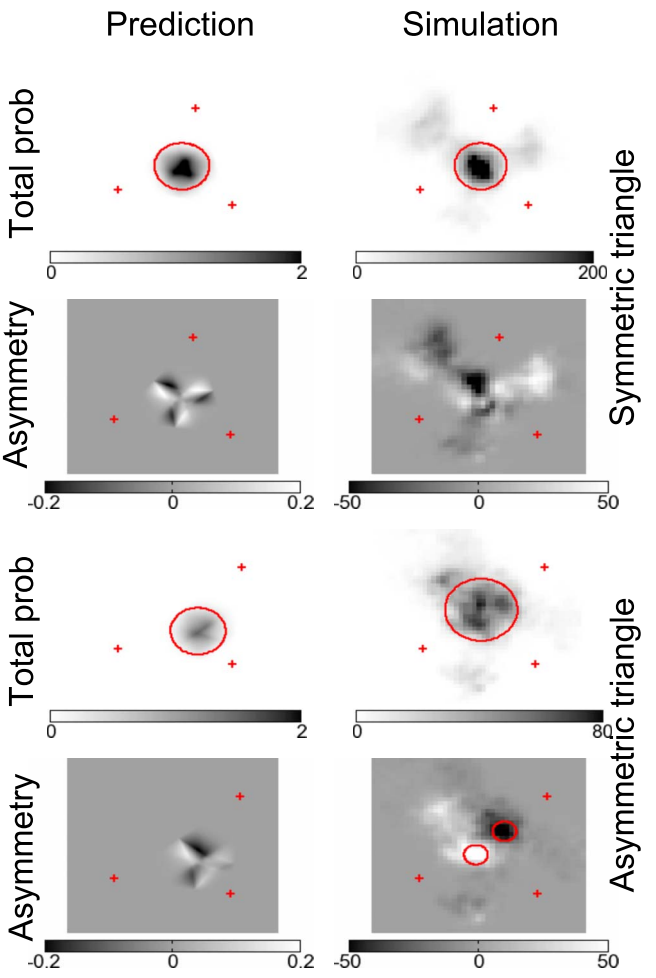

FIG. 6. (Color online) Comparison of predicted and simulated total spiral probability and chirality asymmetry for an almost equilateral and a more asymmetric triangle formed by pacemaker cells (red +) in units of 10^{-5}. In the total probability pictures, black codes for high total probability, while in the asymmetry pictures the colors run from black (exclusively left handed spirals, $A < 0$) over gray (no preference, $A = 0$) to white (exclusively right handed spirals, $A > 0$). Note that in the predictions, the absolute values are scaled down by a factor of 100 because of the different resolution. In the total probability pictures, we integrated over the areas indicated by red circles to get the total spiral probability in the peak areas. In the symmetric triangle, position as well as peak size agree extremely well (simulation: 12.8%, prediction: 11.5%). In the asymmetric case, the peak in the numerical simulations is slightly displaced and washed out, which we assume to be an artifact of coarse graining (note the comparatively large grid point size in the simulations), but the peak size still agrees quite well with our prediction (simulation: 8.4%, prediction: 6.8%). In the chirality asymmetry of the asymmetric triangle, the two red circles indicate areas of almost complete chirality demixing; 92.0% of all spirals found in the bright area are right handed, 92.1% in the dark area left handed.

In the results from the simulations, the total spiral occupancy agrees very well with our prediction. The chirality

asymmetry qualitatively agrees with the prediction as well, but mostly only the strongest expected signals can be observed. This is partly due to the large relative error of a signal gained from subtraction of two noisy quantities and partly due to the slight meandering of spiral tips in the numerical simulation; for the total spiral probability this does not impact the result, but for the asymmetry it is quite noticeable.

Spiral formation of the type described above is also possible from constellations of four or more pacemakers in arrangements similar to equilateral regular polygons. Here, we consider only triangles, since for higher order structures the geometric requirements allowing an inner region of sufficient size and at the same time not separating the structure into several structures of lower order become progressively more restrictive and are less likely to occur. Nevertheless, it is to be expected that higher-order effects have some influence on the situation in more realistic arrangements of pacemakers that we explore in the next section.

V. COMPLEX PACEMAKER PATTERNS

In the preceding section we have shown that our prediction algorithm yields good results when applied to the minimal situation of three pacemakers. We now want to zoom out again to the initial situation of a large cell colony interspersed with many pacemaker cells. Transferring our method is not straightforward, since there is no unique way of partitioning a set of pacemakers into triangles, in fact, there are combinatorially many such triangulations. Since the pacemaker firing pattern is random, one also cannot argue with proximity relations giving rise to connections in a specific order. In light of these complications we opted to not use a unique triangulation, but to sample all relevant pacemaker triangles that could be connected in the neighborhood of each pacemaker, using the following algorithm.

For each pacemaker, calculate the distances to all other pacemakers. Separate the grid area into a fixed number s of equal angle segments centered at the current pacemaker.

Consider all pacemakers as "relevant neighbors" of the current origin that are either closer than a fixed acceptance distance d, or that are the closest one in their angle segment.

Use all triangles that consist of the origin plus any two of his relevant neighbors, that do not contain a further pacemaker within their boundary. This sector sampling algorithm finds triangles including the current origin that could reasonably be formed without being intercepted by other pacemaker regions. For our calculations, we used $s=10$ and $d=4$ for 100×100 grid areas. We used a tenfold magnified version of the grid (1000×1000) when determining spiral probabilities in order to reduce discretization problems with circle intersections, down sampling the result to a 100×100 grid for the correlation coefficient calculations.

Applying the algorithm from Sec. IV to each triangle found in this way yields a fair approximation of the total spiral probability found averaging over one thousand simulations over a range of pacemaker densities. However, we are currently not able to make reliable quantitative predictions about spiral probabilities for complex pacemaker arrangements, because it is nontrivial to decide the relative probabilities and hence weights of overlapping and interdependent triangles in our multitriangulation algorithm. The qualitatively good predictions presented here were obtained with a uniform weight distribution of unity for all triangles, leading to a systematic overestimation of spiral probability.

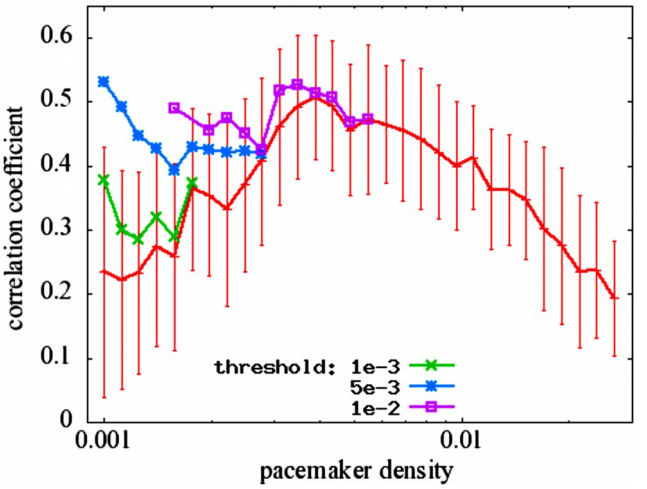

FIG. 7. (Color online) Correlation coefficient between predictions of total spiral probability and corresponding numerical simulations over a range of pacemaker densities (red bottom curve with error bars). No image smoothing was applied. For every density, we considered 20 different realizations of pacemaker patterns, each of which was averaged over 1000 numerical runs. Additional curves show the correlation coefficient when only averaging over runs satisfying an additional minimum peak signal requirement in the spiral occupancy of the numerical simulations in order to avoid artifact dominated runs; these curves are shown for as long as they differ significantly from the red curve. For high pacemaker densities, all runs meet the threshold requirements, and hence the curves collapse onto the solid red curve without thresholds. Error bars of the additional curves are approximately ±0.1 but were omitted for visual clarity.

In order to quantify the quality of our prediction scheme, we calculated the spatial linear correlation coefficient between our predictions and the simulated results. Figure 7 summarizes the quality of our predictions over a range of pacemaker densities. Figure 8 shows examples for the similarity of prediction and numerical results in different areas of the curve.

The decline in predictive power for high pacemaker densities is due to the average distance between neighboring pacemakers becoming too small to support unexcitable inner triangles of the fixed minimal size we require in the prediction algorithm. At the low end of the considered pacemaker density spectrum there is a big spread between pacemaker constellations where the prediction agrees very well to the simulation results, and other constellations, where the simulation results are dominated by artifacts and agreement is almost zero. The low-agreement results can be explained by an artifact already outlined in Sec. II; for very long distances between pacemakers the excitability fronts in our numerical simulations tend to grow in diamond shapes, so that spirals can be formed when two flat excitability fronts meet. To a

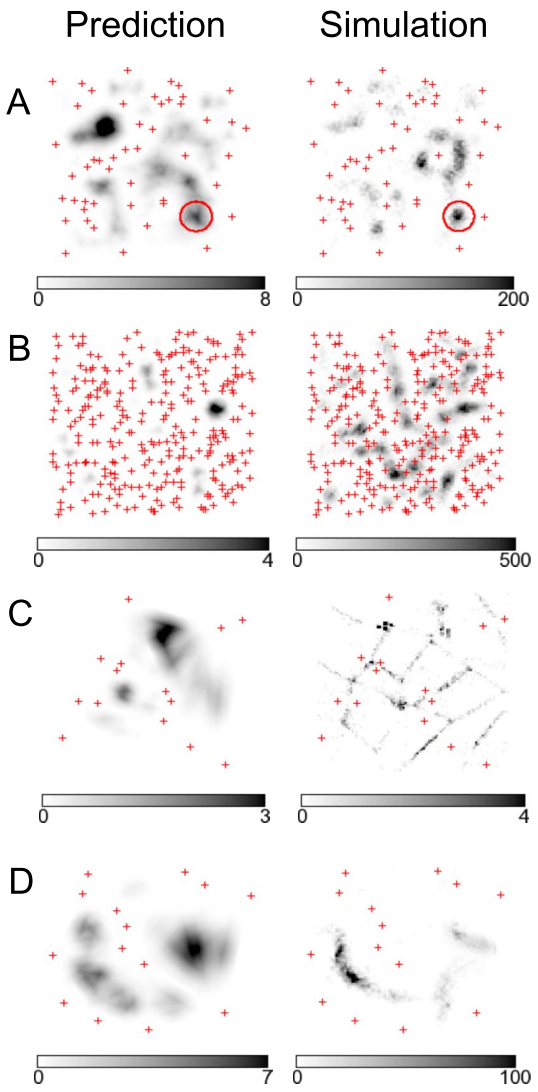

FIG. 8. (Color online) Comparison of predicted and simulated total spiral probability for complex pacemaker arrangements (again, in units of 10^{-5} and the magnitude of the prediction is lowered by a factor of 100 because of differing resolution). Row A shows a pacemaker pattern of intermediate density from near the peak of the correlation curve (ρ=0.0048); the predicted pattern is in close qualitative agreement with the observed average spiral occupancy. Quantitatively, the prediction overestimates the total spiral probability, as outlined in the text; the total probability integrated over the peak indicated by the red circle in the bottom right is 4.7% in the simulations, as opposed to 9.8% according to the prediction. Row B shows a high density pacemaker arrangement (ρ=0.0267); here, only a minority of the observed peaks is predicted correctly, leading to a reduced correlation coefficient. Rows C and D show two realizations of very low pacemaker density arrangements (ρ=0.0014), illustrating the vast differences between single realizations in this regime: in row C the simulation is dominated by artifacts (the similarity to the Voronoi diagram of the pacemakers indicates that mostly only pairs of pacemakers participated in spiral formation) of very low significance and the correlation coefficient between prediction and simulation is close to zero. For the pacemaker arrangement in row D, on the other hand, our prediction shows a high degree of similarity to the numerical simulation, comparable to typical runs from intermediate densities.

small extent, this artifact is present in all simulations, but it is noticeable only if the pacemaker constellation is unsuited for frequent regular spiral formation, which is more likely for low pacemaker densities. Since in most patterns the signals from regular spirals outclass the artifacts by at least one order of magnitude, we experimented with a number of thresholds on the peak signal strength we require for numerical runs to be eligible to enter our average correlation coefficient curve [additional curves in Fig. 7, also see Fig. 8(c)].

Summarizing, our prediction scheme qualitatively performs very well below a critical pacemaker density $\rho_C \approx 0.005$ when discarding numerical runs dominated by artifacts, and correctly predicts some of the peaks in the spiral occupancy for higher densities. We were so far unable to obtain a significantly non-zero correlation coefficient for the handedness asymmetry prediction, although we do observe significant asymmetries in our simulated patterns. We believe the differences to our predictions arise partly from the meandering already quite noticeable in the minimal situation of three pacemakers, and partly from spiral interactions on a larger scale, favoring certain position-handedness constellations and suppressing others.

VI. IMPLICATIONS FOR THE EXPECTED SPIRAL DENSITY OVER FEEDBACK STRENGTH

In earlier simulations, we established that the spiral density over β curve obtained by using fixed pacemakers looks similar to the one shown in Fig. 4(a) of Ref. [10] (where in every time step, a different subset of all cells was checked for random firing). We also found a monotonically rising flank toward higher β, however, we could not observe an increase for very low β values (Fig. 9). Also when using nonfixed (random) pacemakers, the increase in spiral density toward lower β could only be obtained within a very narrow parameter regime (chance to fire per step p_F, selected fraction ϵ). Changing the autonomous excitability increase rate η did not influence the curves significantly, as expected. The fraction ϵ of pacemakers (or chosen cells per time step) was selected to lead to an equal number of expected spontaneous firing events per time, in the following sense: the change in the number of cells able to fire spontaneously in the ready state is

$$\dot{N}(t) = -pN(t) + \frac{N_0 - N(t)}{T_R}, \tag{13}$$

where T_R is the total time needed for recovery and both the recovery and the firing rate are assumed to be quasicontinuous over the population. In the case of fixed pacemakers, the total number of spontaneously firing cells is equal to $N_0 = \epsilon_f N_{\text{total}}$, each of which is selected with probability $p=1$. For the case with randomly selected pacemakers, $N_0 = N_{\text{total}}$ and $p = \epsilon_r$. From the steady-state behavior for both options one can estimate equivalent amounts of pacemakers (or chosen cells), so that one observes a similar number of firing events per time. We used ϵ_f=0.195 for the case with fixed pacemakers, which is equivalent to ϵ_r=0.063 for the case with randomly chosen pacemakers (which produced the closest approximation to the result of Ref. [10]). Having a comparable

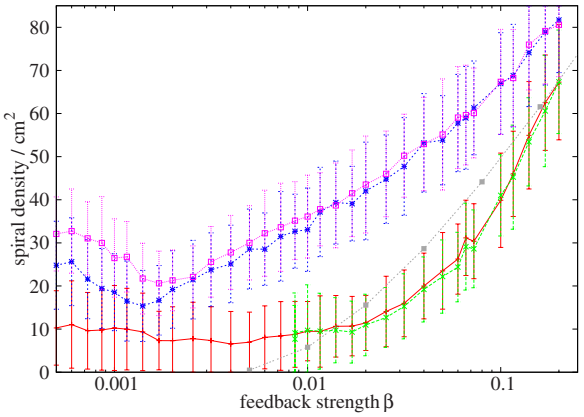

FIG. 9. (Color online) Curves of the spiral density per cm^2 in the asymptotic state. The two upper curves with random pacemakers correspond to the ones shown in Fig. 4 (a) of Ref. [10], with $\eta=5e-4$ [purple (□)] and $\eta=1e-4$ [blue (∗)]. The two lower curves with fixed pacemakers correspond to the simulation protocol we used throughout this paper, with $\eta=5e-4$ [red (+)] and $\eta=1e-4$ [green (×)]. The latter curve was not pursued far below $\beta=0.01$ because of the prohibitive computational effort required to reach the asymptotic state in a sufficient number of simulated runs. The small dependence on η agrees with our proposed mechanism of spiral formation, which should solely depend on beta. Comparing these four curves to our theoretical prediction (brown squares) [for a lower density of fixed pacemakers in the β regime where the radial growth of the excitable areas per firing event can be well approximated by Eq. (10)] reveals a qualitative agreement in scaling for the high β regime. Our prediction has been normalized to coincide with the numerical result for $\beta=0.2$ for fixed pacemakers.

number of spontaneous firing events results in a similar time scale until the asymptotic state is reached, and hence also to a similar influence of the autonomous excitability increase rate η.

We hypothesize that the general shape of the curve has its root in the probability of observing certain firing frequency constellations in a fixed arrangement of pacemakers in our mechanism of spiral formation. By decreasing β, one decreases the radial growth of the excitable regions per firing event [see Eq. (10)], since the excitability rises more slowly in the border areas where cAMP only diffuses to, but is not actively transmitted. This, in turn, increases the average number of firing events required until the excitability fronts meet for a fixed pacemaker triangle geometry. According to our prediction scheme, the higher the number of average firing events, the smaller the relative deviation from the expected case of equal observed firing frequencies. This results in a reduction of the number of triangles that are geometrically eligible to produce spirals at all, since, for roughly equal frequencies (and hence radii of the excitable areas), asymmetric triangles (such as the second example in the previous section) have a too small or no unexcitable inner region where spirals could be formed. For high β on the other hand it takes few firing events for excitable regions to come into contact, and hence the relative spread of realistically observed radius constellations is wider, leading to more pacemaker triangles being able to produce spiral waves.

In Fig. 9 we also show the integrated spiral density prediction for the same complex pacemaker distribution as in Fig. 8(a) (since it describes the real spiral tip occupancy well) over varying β, normalized to agree with our numerical results for a higher pacemaker density with fixed pacemakers at $\beta=0.2$. We expect neither the qualitative nor the quantitative behavior of the pacemaker density over β curve to vary much with changing pacemaker density in the numerical system, since the variant with randomly firing pacemakers case can be considered as the extreme case of a fixed pacemaker density of one, with the effective chance to fire (chance to be selected × chance to fire) tuned down to conserve the expected total frequency of firing events.

VII. CONCLUSIONS

In a recent work, Sawai *et al.* [10] studied spiral tip densities in *Dictyostelium discoideum* colonies as a function of genetic feedback strength. Here we show that not only the density of spiral tips but also their spatial distribution statistically follows certain rules. We developed a scheme to predict the probability distribution of spiral wave tips in a model of cAMP signaling, based on the distribution of a binary characteristic of the cells making up the colony (pacemaker–no pacemaker). It predicts an overall decrease of the spiral density for lower feedback strengths β, consistent with earlier results. This specific prediction scheme is applicable to excitable media with a positive feedback from signal to excitability.

We believe that other mechanics of spiral wave formation will yield different forms of correlations to cell properties. Monitoring inhomogeneities in spiral tip distributions can thus be an important source of evidence for the presence of certain regulatory mechanisms.

On a more general level, with our method it should be possible to predict, how scarred tissue influences the probability of (pathological) spiral wave formation in the heart. It should be noted, however, that for each specific model the main type of correlation has to be checked carefully by numerical simulations.

Beyond the self-organization process in its own right and the fact that, in general, (medium) inhomogeneities tend to favor spiral formation, spiral waves are also advantageous for the system at hand, *Dictyostelium discoideum*, from a biological perspective. In contrast to target waves, they are self-sustained and therefore provide a better (i.e., more robust, more reliable) starting point on the route toward the multicellular aggregate. In essence, target waves—the alternative mode of organizing the cell-to-cell signaling on a larger scale—would require persistent regular pacemaker activity in their center. The establishment, stability, and positioning of a pattern consisting of fully developed spiral waves is thus a vital ingredient in the organism's life cycle. It is therefore easy to understand that the system will have evolved its own internal, single cell-based dynamical mechanisms for generating and establishing a suitable amount of inhomogeneities for spiral wave formation.

The impact of such a distribution of cell properties on the pattern of fully developed spiral waves should be suited for studying a whole range of system features, particularly to

understand how different local interaction mechanisms exploit different cellular properties for establishing this pattern. We believe that such detailed analyses will give insight into the biological mechanisms evolved for establishing inhomogeneities in the system. Here, however, our aim was to establish and discuss the general phenomenon of pattern predictability from cell properties. Therefore, we selected a cell property, which is binary and biologically plausible: the capacity of a cell to yield spontaneous firing events.

ACKNOWLEDGMENTS

This work was funded by Deutsche Forschungsgemeinschaft, Project No. HU 937/4-2.

[1] A. S. Mikhailov and V. Calenbuhr, *From Cells to Societies* (Springer, Berlin, 2006).
[2] J. Lauzeral, J. Halloy, and A. Goldbeter, Proc. Natl. Acad. Sci. U.S.A. **94**, 9153 (1997).
[3] H. Levine, I. Aranson, L. Tsimring, and T. V. Truong, Proc. Natl. Acad. Sci. U.S.A. **93**, 6382 (1996).
[4] E. Pálsson, K. J. Lee, R. E. Goldstein, J. Franke, R. H. Kessin, and E. C. Cox, Proc. Natl. Acad. Sci. U.S.A. **94**, 13719 (1997).
[5] M. I. Rabinovich, A. B. Ezersky, and P. D. Weidman, *Dynamical Theory of Pattern Formation* (World Scientific Publishing Company, Singapore, 2001).
[6] R. H. Kessin, *Dictyostelium: Evolution, Cell Biology, and the Development of Multicellularity, Developmental and Cell Biology Series* (Cambridge University Press, Cambridge, 2001).
[7] B. Vasiev and C. J. Weijer, Biophys. J. **76**, 595 (1999).
[8] D. Dormann, J.-Y. Kim, P. N. Devreotes, and C. J. Weijer, J. Cell. Sci. **114**, 2513 (2001).
[9] D. A. Kessler and H. Levine, Phys. Rev. E **48**, 4801 (1993).
[10] S. Sawai, P. A. Thomasson, and E. C. Cox, Nature (London) **433**, 323 (2005).
[11] A. Samadani, J. Mettetal, and A. van Oudenaarden, Proc. Natl. Acad. Sci. U.S.A. **103**, 11549 (2006).
[12] K. J. Lee, Phys. Rev. Lett. **79**, 2907 (1997).
[13] R. A. Gray, A. M. Pertsov, and J. Jalife, Nature (London) **392**, 75 (1998).
[14] M.-A. Bray, S.-F. Lin, R. R. Aliev, B. J. Roth, and J. P. Wikswo, J. Cardiovasc. Electrophysiol. **12**, 716 (2001).
[15] K. J. Lee, E. C. Cox, and R. E. Goldstein, Phys. Rev. Lett. **76**, 1174 (1996).
[16] A. T. Winfree, *When Time Breaks Down: The Three-Dimensional Dynamics of Electrochemical Waves and Cardiac Arrhythmias* (Princeton University Press, Princeton, 1987).
[17] J. P. Keener, J. Math. Biol. **29**, 629 (1991).